Journal of Power Sources 227 (2013) 229–236

Contents lists available at SciVerse ScienceDirect

Journal of Power Sources

journal homepage: www.elsevier.com/locate/jpowsour

Improvement of proton exchange membrane fuel cells performance by coating hygroscopic zinc oxide on the anodic catalyst layer

Rong-Hsin Huang [a], Tsai-Wei Chiu [a], Tien-Jen Lin [a], Chung-Hsing Sun [a], Wen-Kai Chao [a], Du-Cheng Tsai [a], Kan-Lin Hsueh [b], Fuh-Sheng Shieu [a,*]

[a] Department of Materials Science and Engineering, National Chung Hsing University, Taichung 40227, Taiwan
[b] Department of Energy Engineering, National United University, Miaoli 36003, Taiwan

HIGHLIGHTS

- Low-amount hygroscopic ZnO can be prepared by sputtering deposition.
- ZnO nanoparticles were well coated on the catalyst layer by sputter deposition.
- ZnO quantity controlled the wettability of the ZnO/PtC anode catalyst layer.
- MEA exploit with ZnO (0.46 and 0.53 wt.%) addition was better than that without ZnO.
- MEA30 capacity was 43.91% higher than that of MEA0 at 45 °C anode temperature.

ARTICLE INFO

Article history:
Received 22 August 2012
Received in revised form
11 November 2012
Accepted 13 November 2012
Available online 23 November 2012

Keywords:
Zinc oxide nanoparticle
Proton exchange membrane fuel cells
Wettability
Sputtering deposition method

ABSTRACT

This study proposes that hygroscopic zinc oxide (ZnO) nanoparticles, added to the anodic catalyst layer as a water adsorbent by using sputtering deposition, improves the hydration of the anode under dehydrated conditions, thereby enhancing the performance of proton exchange membrane fuel cells (PEMFCs). Scanning electron microscopy analysis indicates that the size of the ZnO nanoparticles ranges between 5 nm and 20 nm on the Si-substrate and aggregates on the platinum/carbon (PtC) catalyst layer with ZnO. The ZnO content of the ZnO/PtC catalyst is estimated by inductively coupled plasma-atomic emission spectra. Water contact angle analyzes show the hydrophilicity of the ZnO/PtC catalyst. Single cell performance with various amounts of ZnO nanoparticles in the anode catalyst layer is investigated at the anode humidifier temperatures of 25 °C, 45 °C, and 65 °C. The cell and cathode humidifier temperatures are fixed at 60 °C and 65 °C, respectively. The membrane-electrode assembly (MEA30) with 0.45 wt.% ZnO in the anode catalyst layer revealed the best performance at anode humidifier temperatures 45 °C and 65 °C, with power densities 43.91% and 25.80% higher than those without ZnO, respectively. The results show that anode catalysts with proper hygroscopic ZnO nanoparticles are ideal for PEMFCs applications.

1. Introduction

Proton exchange membrane fuel cells (PEMFCs) have near-zero pollutant emission, high power density, high energy conversion efficiency, and simple operation that far exceed those of conventional internal combustion systems using fossil fuels [1–3]. In the past decade, PEMFCs have been recognized as the most promising candidates for a wide range of applications in transportation as well as home and portable devices [4,5]. Considerable efforts have been exerted to commercialize PEMFCs. However, the drying and flooding phenomena of a membrane electrode assembly (MEA) under a dehydration environment still influence the performance of PEMFCs. The drying phenomenon of the Nafion® membrane and anodic catalyst layer dehydration negatively affect the proton conductivity, which results in the degradation of cell performance. Pt activity in the anode catalyst layer is also easily decreased by CO poisoning under a low humidification condition, resulting in reduced cell performance and life [6–8]. To overcome these problems, a capable MEA that can maintain an optimum hydration level under dehydration conditions without the assistance of an external humidifying system is desired.

* Corresponding author. Tel.: +886 4 2285 4563; fax: +886 4 2285 7017.
E-mail addresses: fsshieu@dragon.nchu.edu.tw, D9666210@mail.nchu.edu.tw (F.-S. Shieu).

0378-7753/$ – see front matter © 2012 Elsevier B.V. All rights reserved.
http://dx.doi.org/10.1016/j.jpowsour.2012.11.036

Nafion® membrane, a core unit of the MEA, supports the hydrogen proton transmission from anode to cathode. A satisfactory hygroscopic ability of Nafion® membrane results in cell performance maintenance, life extension, and Pt CO poisoning resistance. Considerable efforts have been exerted to modify MEA into being able to maintain its appropriate wettability to solve the aforementioned dehydration issues. Several admirable syntheses have been carried out; for example, organic–inorganic composite membranes have been prepared by combining hygroscopic metal oxide particles such as ZrO_2, SiO_2, TiO_2, WO_3, and ZrP with Nafion® resin to maintain the proper hydration level in electrodes under low-humidity conditions [9–16]. Acid composite membranes have been synthesized by combining solid acids and heteropoly acids such as sulfonated ZrO_2, phosphotungstic acid, and molybdophosphoric acid to increase the acid sites that promote local migration and improve proton conductivity [17–20]. The cathode gas diffusion layer (CGDL) modification improves the cell performance under suitably humidified condition. Williams et al. [21] reported the proper CGDL combination of TGPH-120 carbon paper (Toray Corporation, Japan) as macro-porous substrate, Vulcan XC-72R, and 14% polytetrafluorethylene, and Lee et al. [22] reported using Fluorocarbon material to modify CGDL. Both reports showed improvement in cell performance. By adding hygroscopic materials such as SiO_2, clay, γ-Al_2O_3, TiO_2, and AB_2-type hydrogen storage alloy to the hygroscopic composite anode catalyst layer of a MEA, its wettability and performance under low-humidity conditions can be improved [23–29]. Nevertheless, these hygroscopic materials easily lead to agglomeration by the improper handing of the catalyst layer in blocking the fuel pathway and increase the internal resistance of the MEA. Consequently, the performance of MEA is negatively affected. This viewpoint has been reported by Dai et al. [16]. Thus, the agglomeration and proper amount of hygroscopic metal oxide nanoparticles on the anode catalyst surface need to be decreased, and the MEA wettability needs to be simultaneously maintained to obtain a versatile MEA capable of maintaining the optimum hydration level under dehydration conditions.

Metal oxides are widely investigated as water molecule absorbents that can be added to the anode catalyst layer to enhance the MEA wettability. In particular, zinc oxide (ZnO) is advantageous given its easy availability, facile synthesis, low cost, advanced characteristics, and natural richness. ZnO and ZnO-based admixture catalyst materials have been extensively investigated for their uses in the methanol steam reforming of PEMFCs [30–35]. A large number of studies have reported the hydrophilic characteristics of ZnO materials [36–38]. However, there are relatively few studies focusing on the uniform distribution of hygroscopic ZnO nanoparticles on the surface of the platinum/carbon black (PtC) anode catalyst layer by the sputtering technique, and its effects on the performance of PEMFCs. The present study investigates the feasibility of coating a few uniformly distributed hygroscopic ZnO nanoparticles on the anodic PtC catalyst layer surface by the direct current sputter deposition system. ZnO nanoparticles were used as water adsorbents due to the Lewis acid sites distributed all over their surface, which maintain the optimum anode hydration level under dehydration conditions. The ZnO nanoparticles were characterized by X-ray diffraction (XRD), scanning electron microscopy (SEM), and transmission electron microscopy (TEM). Three critical factors of the anodic ZnO/PtC catalyst layer, namely, wettability, electrical resistance, and ZnO/PtC particle loading, were also studied. A polarization test was conducted to investigate the influence of the anodic PtC catalyst layer with the hygroscopic ZnO nanoparticles at different anode humidifier temperatures (25, 45, and 65 °C) on the cell performance. The temperatures of the cell and cathode humidifier were both fixed at 60 °C. The polarization measurement was conducted at ambient conditions.

2. Experimental

2.1. Preparation of the PtC and ZnO/PtC catalyst material

PtC (20 wt.%) catalyst was synthesized by the impregnation method [23,26]. The natural inorganic mineral of sodium montmorillonite (Nancor, USA) was first used to disperse carbon black (CB; Vulcan® XC-72, Cabot) in distilled water. The mixture was then ultrasonicated for 2 h to obtain finely dispersed CB particles. Thereafter, the platinum precursor (H_2PtCl_6 $6H_2O$; Alfa Aesar, 99.95%), 10 mL of 1 M NaOH, and 10 mL of 99.8% methanol (EM-1001, ECHO, Chemical Co., Ltd.) were added to the aforementioned mixture, and stirred at 80 °C for 4 h to disperse the PtC catalysts well. The as-made PtC catalysts were filtered and dried in a vacuum oven under a pressure of 101.32 Pa at 80 °C for 6 h.

Zinc oxide (ZnO) nanoparticles were prepared by the physical vapor deposition (PVD) direct current (DC) sputter system. The operation parameters are listed in Table 1. The as-made PtC catalyst layer, as a substrate, was prepared with 20 wt.% PtC catalyst, 5 wt.% Nafion solution (DuPont), and alcohol (98%, Aldrich) mixed using an ultrasonator for 1 h. The mixture was sprayed onto the commercial hydrophobic carbon clothes (Beam Associate Co., Ltd.). The hydrophilic electrode material (ZnO/PtC) was prepared by sputtering the ZnO nanoparticle coating on the as-made PtC catalyst layer. The preparation times of the ZnO/PtC catalyst layer were 30, 60, and 90 s, and the resulting samples were labeled as ZnO/PtC-30 s, ZnO/PtC-60 s, and ZnO/PtC-90 s, respectively.

2.2. Characterizations of the ZnO/PtC catalyst material

The crystal structure of the Pt nanoparticles was analyzed using a MAC MXP III X-ray diffractometer with Cu Kα radiation ($\lambda = 0.154$ nm, sweeping angle of $2\theta = 10°–90°$, sweeping rate of $2°min^{-1}$). The diffraction peaks were compared with those in the JCPDS data file. The morphology and distribution of Pt and ZnO nanoparticles on the PtC catalyst material were examined using a field emission SEM (FE-SEM) system (JEOL 6700, Japan). The distribution of ZnO nanoparticles on the glass substrate and selection area diffraction (SAD) of the ZnO crystal structure were estimated by a field emission TEM (FE-TEM) system (JEOL 2100F, Japan) operating at 200 kV. The wettability of ZnO/PtC catalyst was determined by the sessile drop method (First Ten Angstro, FTA 2000, USA). In addition, some of the ZnO/PtC nanoparticles obtained from the top catalyst layer of the carbon cloth were mixed with dry potassium bromide (KBr) powders (ZnO/PtC:KBr = 1:100) to press a disc for Fourier-transform infrared (FTIR, Spectrum RXI, Perkin Elmer, U.S.A.) analysis in the diffuse reflectance mode. The dried KBr was heated in a furnace overnight at 130 °C to minimize the amount of the adsorbed water. FTIR was used to detect the hydrophilic group (–OH) of the ZnO/PtC nanoparticles adsorbed on

Table 1
Parameters of the sputtered ZnO nanoparticles on the PtC catalyst layer.

Target	ZnO
Substrate	Carbon cloth (with PtC on it)
Base pressure	1.0×10^{-5} torr
Working pressure	1.5×10^{-3} torr
DC power	125 W
Ar	10 sccm
Working distance	5 cm (holder location)
Sputtering time	30, 60, 90 sec
Operation temperature	Room temperature

the nanoparticle surface. The weight percentages of ZnO in the ZnO/PtC catalysts were measured by inductively coupled plasma-atomic emission spectrometry (ICP-AES) system (ICAP 9000, Jarrell-Ash, USA).

2.3. Measurement of polarization curves

The hydrophilic ZnO/PtC catalyst served as the anode catalyst layer. The cathode was maintained by the PtC catalyst. A Nafion 112 membrane (DuPont) was sequentially pretreated with 5 wt.% H_2O_2 (Aldrich), deionized (DI) water, 1.0 M H_2SO_4 (Aldrich), and DI water at 80 °C for 1 h. Thereafter, the Nafion 112 membrane was used as a separator for the anode and cathode, and hot-pressed under 100 kgf cm^{-2} at 100 °C for 3 min. The Pt loading at both anode and cathode was 0.4 mg cm^{-2}, and the effective area of each MEA was 5 cm^2.

The hydrophilicity of the ZnO/PtC-30 s, ZnO/PtC-60 s, and ZnO/PtC-90 s anode catalyst materials combined with the no-ZnO nanoparticle PtC cathodes labeled as MEA30, MEA60, and MEA90, respectively, was examined. The anode and cathode catalyst layers of MEA0 had PtC catalysts without ZnO nanoparticles. The polarization curves of the MEAs were obtained using a fuel cell workstation (Beam Associate Co., Ltd.). Hydrogen and oxygen were provided to both the anode and cathode at a streaming rate of 50 sccm. The performances of the MEAs were characterized under a potential sweep rate of 0.56 V min^{-1} at the anode humidifier temperatures of 25, 45, and 65 °C using a fuel cell workstation. The temperatures of the cell and cathode humidifier were maintained at 60 and 65 °C, respectively. The polarization test was performed under ambient conditions.

3. Results and discussion

3.1. Characterization of the ZnO/PtC catalyst

Fig. 1 shows the wide-angle XRD spectra of the 20 wt.% PtC and ZnO/PtC catalysts. The diffraction peaks of Pt were observed at $2\theta = 39.85°$, 46.19°, 67.74°, and 81.52°, corresponding to the crystalline planes of Pt at (111), (200), (220), and (311), respectively, compared with the JCPDS data file (No. 04-0802). At $2\theta = 31.74°$ and 36.4°, the diffraction peaks of ZnO were demonstrated to correspond to the crystalline planes of ZnO at (100) and (101), respectively, compared with the JCPDS data file (No. 89-1397). At $2\theta = 37.05°$ and 41.55°, ZnO_2 diffraction peaks corresponding to the ZnO_2 crystalline planes (200) and (210), respectively, were observed. The XRD patterns show that Pt in the catalyst has a face-centered cubic structure, and ZnO nanoparticle has a hexagonal structure. The existing ZnO_2 composition was ascribed to the oxidation of the sputtered ZnO nanoparticle easily occurring under ambient conditions.

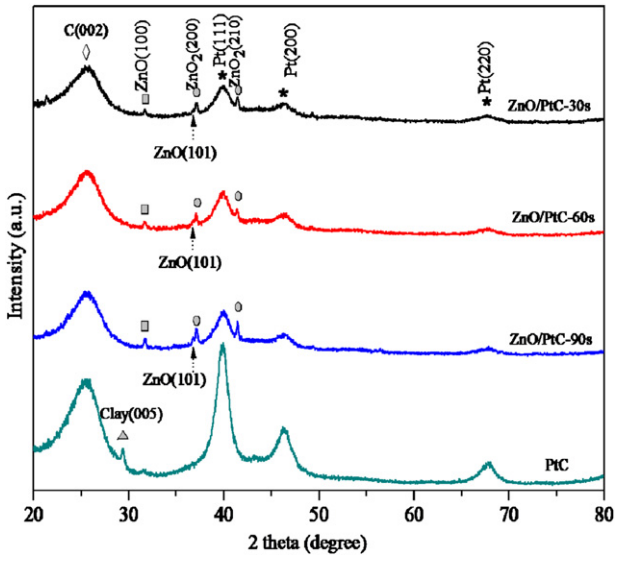

Fig. 1. Wide-angle XRD spectra of 20 wt.% PtC, ZnO/PtC-30 s, ZnO/PtC-60 s, and ZnO/PtC-90 s catalysts.

Fig. 2 shows the FE-SEM images of the ZnO/PtC catalysts and the ZnO-coated Si substrate with various sputtering times. The spherical morphology and good dispersion of Pt nanoparticles on the surface of CB can be seen in Fig. 2a. The agglomeration of the spherical ZnO nanoparticles increased along with the amount of ZnO nanoparticles coated on the PtC catalyst layer, as demonstrated in Fig. 2b–d. The size of the aggregated ZnO particles ranges from 25 nm to 100 nm. For comparison, the ZnO nanoparticles were coated on the Si substrate as a reference. The size and aggregation of the ZnO nanoparticles on Si substrate increased with increasing deposition time, as shown in Fig. 2e–g. The size of the ZnO nanoparticle spans from 5 nm to 20 nm. The agglomeration of the ZnO nanoparticles on the PtC catalyst layer is quite similar to that on the Si substrate. However, the particle size of ZnO on the Si substrate is smaller than that of ZnO on the PtC catalyst layer, which was presumably attributed to be influenced by the roughness of the substrate. Fig. 3a shows the TEM image of the in-house PtC catalyst, indicating that the Pt nanoparticles in the PtC catalyst were well dispersed on CB. The Pt nanoparticle sizes were estimated to range from 3.5 nm to 18 nm. Fig. 3b shows the TEM image of the ZnO nanoparticle coating on the silica substrate (30 s coating time). The SAD pattern of ZnO in Fig. 3c illustrates the hexagonal structure of the ZnO nanoparticles, consistent with the XRD results.

3.2. Pt and Zn contents in the ZnO/PtC catalyst

The Pt and Zn contents of the ZnO/PtC catalyst were first determined by ICP-AES before obtaining the polarization curve of the MEA with the ZnO/PtC catalyst layer in the anode. The results are summarized in Table 2. The Pt content in the ZnO/PtC catalyst was maintained at ca. 59.3 ± 1.3 ppm. The Zn content in the ZnO/PtC catalyst increased with increased sputtering times (1.11, 1.24, and 1.74 ppm to 30, 60, and 90 s). The ZnO content and weight percentage in the ZnO/PtC catalyst were estimated by stoichiometry. The calculation results are listed in Table 2.

3.3. Hydrophilicity of the ZnO/PtC catalyst layer

The hydrophilic characteristic of the ZnO/PtC catalyst layer in the anode of MEA was investigated to confirm the wettability of the ZnO/PtC catalyst layer. Fig. 4 shows the images of water droplets on the catalyst layers with various samples of ZnO/PtC catalysts. The average water contact angles of ZnO/PtC-30 s, ZnO/PtC-60 s, and ZnO/PtC-90 s were found to be 41.17°, 33.08°, and 13.75°, respectively. The water contact angle decreased with increased amount of ZnO nanoparticle. The wettability of the added ZnO nanoparticle catalyst layer differed obviously from that of the PtC catalyst layer and was strongly related to the amount of added ZnO nanoparticle. Comparisons with the results of previous studies adding SiO_2, TiO_2, and γ-Al_2O_3 particles to the catalyst layer [24,26–28] reveal that ZnO nanoparticles exhibit better wettability than these oxides for low addition amounts. The results indicate that the sputtering manner of the added water molecule adsorbent coating on the surface catalyst layer was better than the mixture on the catalyst layer.

Furthermore, the hydrophilic functional group (-OH) of the ZnO/PtC catalysts surface (contained the ZnO/PtC-30 s, ZnO/PtC-60 s,

and ZnO/PtC-90 s samples) was demonstrated by the FTIR, by which it is demonstrated that the ZnO/PtC catalysts have the Lewis acid sites. Fig. 5 shows that the peaks of the (−OH) group and the hydrophobic group (C—H) were observed at 3200–3600 nm and 2850–2960 nm, respectively. Compared with the two peaks, the intensity of the hydrophilic group (−OH) increased with increased amount of ZnO, signifying hydrophilic addition. This result agreed with that of the water contact angle of the ZnO/PtC catalyst, thereby assistance confirming that the wettability of the ZnO/PtC catalyst layers can be improved by ZnO nanoparticle addition.

3.4. Single-cell polarization test

The ideal water management can improve the MEA performance. In the single-cell polarization test, the polarization curves of four different MEAs were performed at various anode humidifier temperatures (25, 45, and 65 °C), as shown in Fig. 6a–c, respectively. Both cell and cathode humidifier temperatures were maintained at 60 and 65 °C, respectively. Table 3 lists the maximum current density and power density of these MEAs.

Fig. 6a shows that at the cell voltage of 0.6 V under an anode humidification temperature of 25 °C, the order of the current density was MEA60 > MEA30 > MEA90 > MEA0. This result indicated that the hygroscopic characteristic of the ZnO nanoparticles adsorbs the water molecule, from the back diffusion of water vapor, to increase the wettability of the anode catalyst layer. Thereby, the MEA performance was improved under low humidification. MEA60 exhibited the best performance among the MEAs. The result suggested that the proper water molecule absorbability of MEA affected its performance. The results of the water contact angle analysis demonstrated that the anode hygroscopic ability of MEA60 was better and lower than that of MEA30 and MEA90, respectively. The low water molecule absorbability of MEA30 did not maintain the suitable wettability of the proton exchange membrane [39–41]. The high water molecule absorbability of MEA90 and the movable route of fuel in the gas diffusion layer were likely blocked by the overflow water. The Zn^{2+} ions could be more easily exchanged with the sulfonic groups in contact with the Nafion membrane to reduce its proton exchange capacity under the watery condition. The three phenomena did not enhance MEA performance. According to previous speculation, the hygroscopic characteristic ZnO nanoparticles added to the anode catalyst layer is not a main factor for improving the cell performance because if so, then the cell performance should be enhanced with increased amount of ZnO nanoparticle additive. Fig. 6b shows the polarization curves with the anode humidification temperatures at 45 °C. The current density of the MEAs at the cell voltage of 0.6 V followed the order of MEA30 > MEA60 > MEA0 > MEA90. MEA30 exhibited the highest current density among the MEAs at 45 °C. The excessive amounts of ZnO nanoparticles added to the MEA60 and MEA90 (0.53 wt.% and 0.71 wt.%, respectively) could easily aggregate on the catalyst layers and absorb more water molecules to block the transport route of the fuel or protons, and thus created higher internal resistance. As a result, the phenomenon of Zn^{2+} ions exchanging with the sulfonic groups of MEA90 became more serious. These factors could cause the decreased cell performance under the humidity condition, by which MEA90 led to the worst performance. Furthermore, a higher humidity in anode was provided through a higher anode

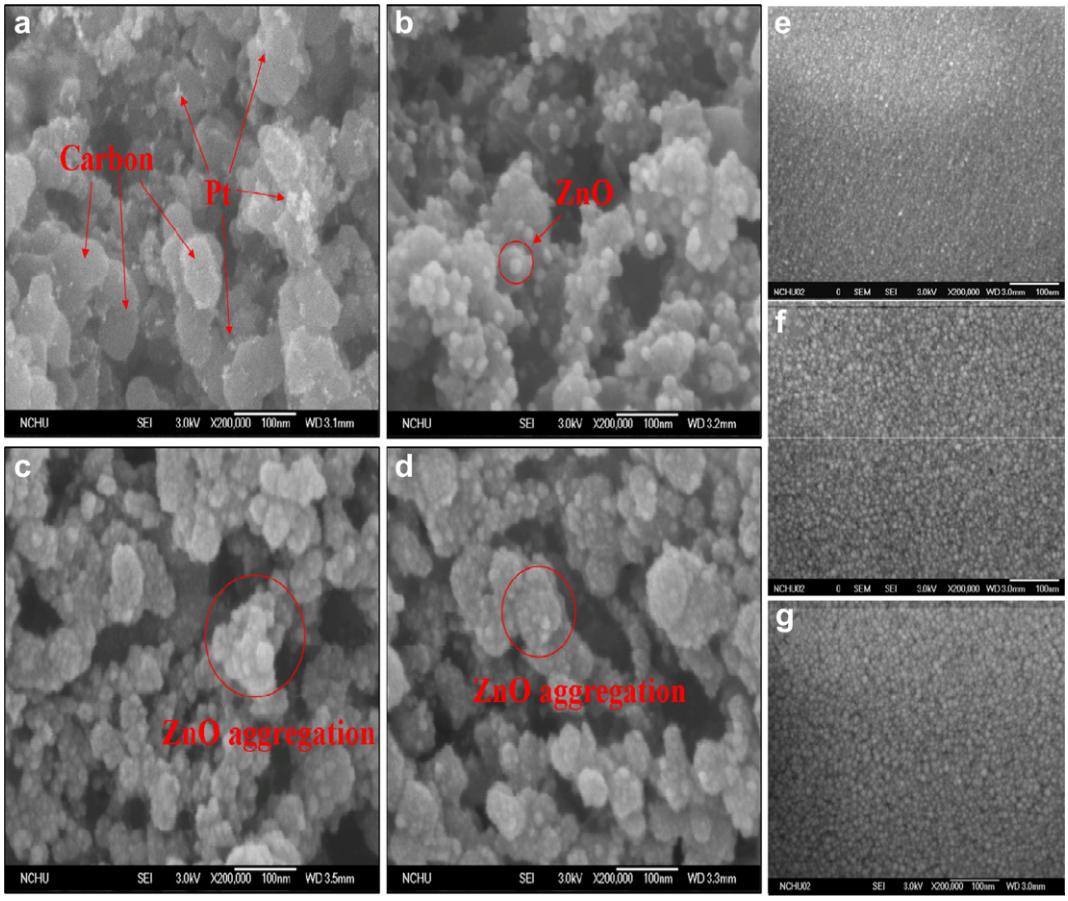

Fig. 2. FE-SEM images of (a) 20 wt.% PtC, (b) ZnO/PtC-30 s, (c) ZnO/PtC-60 s, and (d) ZnO/PtC-90 s catalysts. The content of other SEM images are (e) ZnO/Si substrate-30 s, (f) ZnO/Si substrate-60 s, and (g) ZnO/Si substrate-90 s.

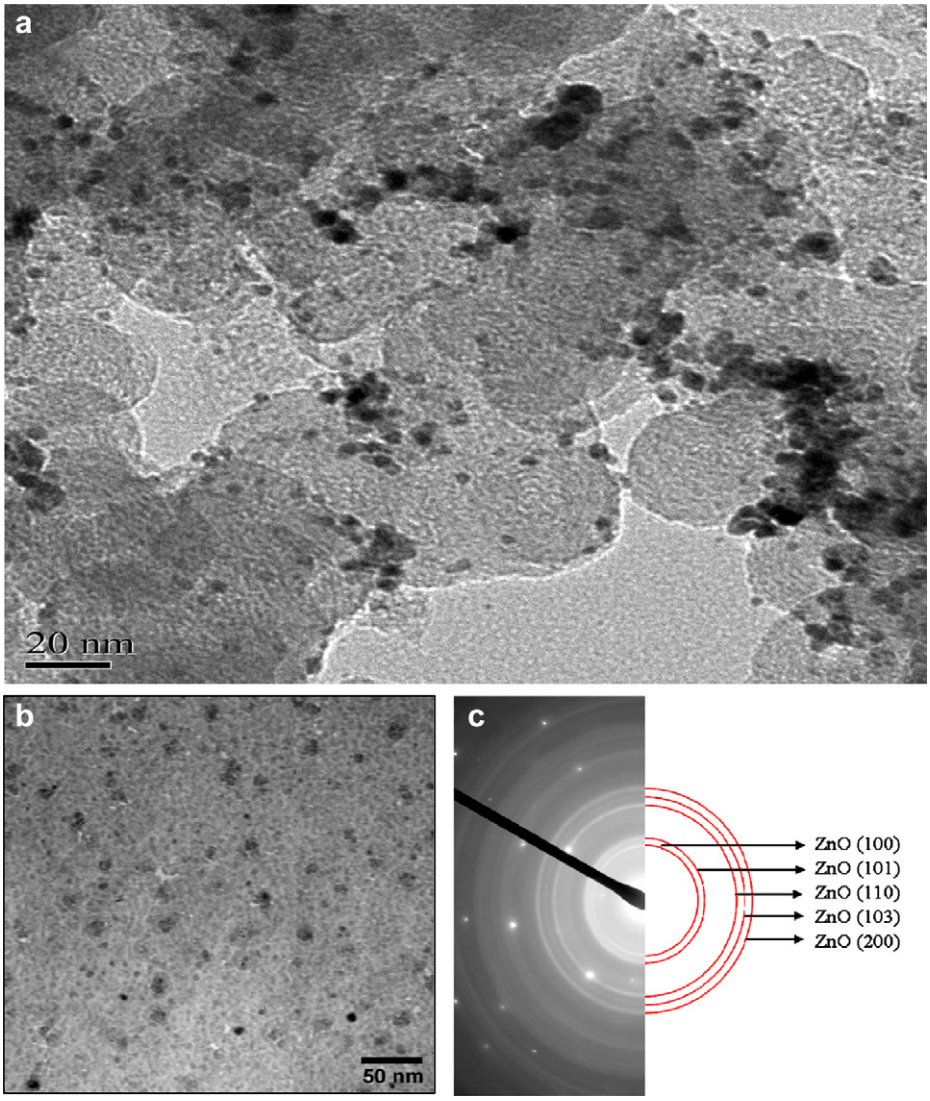

Fig. 3. TEM micrographs of (a) 20 wt.% PtC and (b) ZnO/SiO_2 (substrate). (c) Selected area diffraction of ZnO nanoparticles.

humidification temperature. At a cell voltage of 0.6 V, the current density with an anode humidification temperature of 45 °C was higher than the current density at 25 °C, especially the MEA30, which shows a nearly 0.1 A cm^{-2} increase in current density. Fig. 6c shows the polarization curves of the MEAs with the anode humidification at 65 °C (fully humidified condition), whose the current density followed the order MEA60 > MEA30 > MEA0 = MEA90 in a small current density (voltage above 0.6 V). The performances of the MEA30 and MEA60 with the anode low humidification (45 °C) to fully humidified condition (65 °C), which were improved 0.12 A cm^{-2} and 0.05 A cm^{-2} at 0.6 V, respectively. The result indicates that the humidification ability of the positive catalyst layer of the MEA60 was better than that of the MEA30. Hence, the hygroscopic ZnO/PtC-60 s catalyst could increase the ion conductivity to improve the cell performance even more than that of the hygroscopic ZnO/PtC-30 s catalyst. The performance of the MEA90 was remarkably decreased as a result of the flooding condition and the poisoned sulfonic groups.

Table 2
Pt and Zn contents in the ZnO/PtC catalysts and weight percentage of ZnO in ZnO/PtC.

Catalyst samples	Pt (ppm)	Zn (ppm)	ZnO (ppm) by stoichiometry estimate	The weight percentage of ZnO in ZnO/PtC (wt.%)
ZnO/PtC-30 s	60.2	1.11	1.38	0.46
ZnO/PtC-60 s	58.1	1.24	1.54	0.53
ZnO/PtC-90 s	60.6	1.74	2.17	0.71

From the polarization curves in Fig. 6a–c, the activation polarization zone clearly indicates that the hydrogen oxidation reaction is facile because of the improvement in the wettability of electrocatalyst layer with 3-D structure by the anode humidification and the water back diffusion from the cathode. A typical expression for the cell voltage E_{cell} is given by Yousfi-Steiner et al. [42]. The equation (1) could be used to explain which term had been improved in the humidified condition.

$$E_{cell} = E_r^o - \eta_{a,act} - \eta_{c,act} - \eta_{iR} - \eta_{a,conc} - \eta_{c,conc} \quad (1)$$

where E_r^o is the standard electromotive potential of the cell, $\eta_{a,act}$ the anode activation over-potential, $\eta_{c,act}$ the cathode activation over-potential, η_{iR} the internal resistance over-potential, $\eta_{a,conc}$ the anode concentration over-potential, and $\eta_{c,conc}$ the cathode concentration over-potential. Humidification level of the cell affects

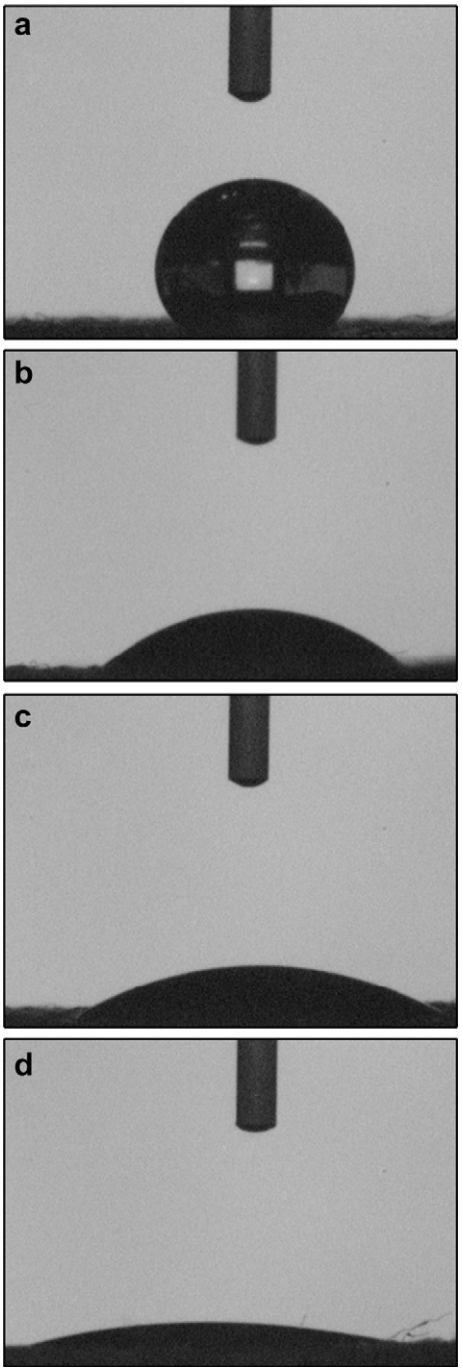

Fig. 4. Contact angle measurement using water droplets on the ZnO/PtC catalyst layers; (a) PtC, (b) ZnO/PtC-30 s, (c) ZnO/PtC-60 s, and (d) ZnO/PtC-90 s.

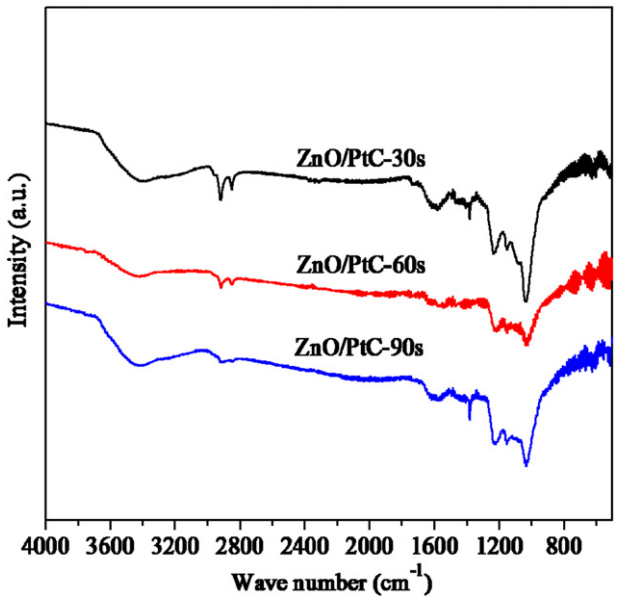

Fig. 5. FTIR curves of (a) ZnO/PtC-30 s, (b) ZnO/PtC-60 s, and (c) ZnO/PtC-90 s catalysts.

the ionic conductivity of the anode, cathode, and membrane. The facile proton and water migration reduce the loss of activation and internal over-potential and thus improve the performance of the single cell. This means that $\eta_{a,act}$, $\eta_{c,act}$, and η_{iR} are subject to the influence of the cell humidification in above 0.6 V.

In a large current density (voltage below 0.6 V), the current density followed the order MEA30 > MEA60 > MEA0 = MEA90, as shown in Fig. 6(c). The current density at cell voltages below 0.6 V was mainly affected by ohmic and concentration polarization losses. To achieve suitable wettability for an anodic catalyst, the ionic resistance of a single cell needs to be reduced [28,29]. However, the excess ZnO nanoparticles aggregated, had high resistance, and poisoned the sulfonic groups. As a result, the excess ZnO nanoparticles hindered ion migration and increased the ionic resistance. They also block the diffusion of hydrogen and water vapor to extend the distance of the gas diffusion route, thereby worsening the entire reaction rate and cell performance. Therefore, the performance of MEA30 was better than those of MEA60 and MEA90. For higher hydration levels, the wettability of the anode activity catalyst layer can be achieved at a higher anode humidification temperature, as reported by B. M. Mahan and R. J. Myers [43]. The saturation pressure of water vapor rapidly increases from 50 °C. The amount of water in the anode provided by the anode humidifier set at 65 °C was much higher than that at 25 and 45 °C. Table 4 listed the saturation pressure of water vapor at 25, 45, and 65 °C. For MEA90, the negative effect caused by the higher ZnO nanoparticle content increased and the positive influence that induced the better wettability of the catalyst layer improved. The current density of MEA90 decreased with increased anode humidifier temperature, and then decreased to become lower than that of MEA0 at the anode humidifier temperature of 65 °C. This phenomenon indicated water flooding at the anode, which accumulated excess water within the channels of the bipolar plate.

The cell performance of the ZnO nanoparticles added to a MEA is mainly determined by a competition mechanism containing the positive effect caused by the enhanced wettability of the anodic catalyst layer, the negative effect induced by the aggregation and intrinsic resistance of the excessive ZnO nanoparticles, and the probable poisoning of the sulfonic groups of the Nafion membrane caused by the Zn^{2+} ions. The combination effect of ZnO nanoparticle addition to the internal cell resistance was studied. The internal cell resistance could be regarded as the sum of the ionic resistance of the membrane, ionic resistance of the ionomer in the catalyst layer, and electrical resistance of the ZnO particles. Ionic resistance was affected by the wettability of the anode catalyst layer and the amount of water provided by the anode humidifier. The electronic resistance of the anode catalyst layer was determined by the added amount of ZnO nanoparticles. A simplified semi-empirical equation (2) given by Tu et al. [44] was adopted to estimate the internal resistance of the single cell from the polarization curves.

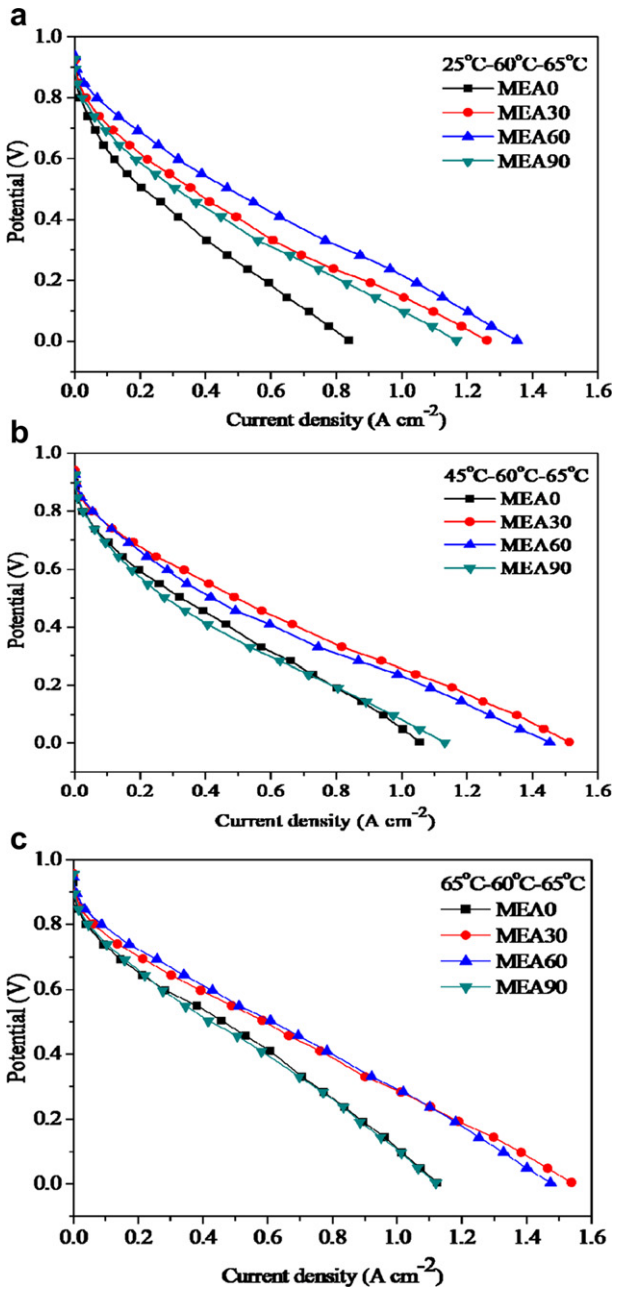

Fig. 6. Polarization curves of MEAs at different anode humidifier temperatures of (a) 25, (b) 45, and (c) 65 °C with the cathode humidifier and cell temperatures kept at 65 and 60 °C, respectively.

$$E = A - B \times \ln i - R \times i \quad (2)$$

where R equals to the internal cell resistance, $R{\cdot}i$ denotes the internal resistance over-potential as given by η_{iR} is equation (1), while B is an overall Tafel slope. The $B \times \ln i$ is equivalent to the electrode activation overpotential ($\eta_{a,act} \pm \eta_{c,act}$) in equation (1). A is a constant depending on E_r^o and the exchange current density. The presumable value of electrode resistance is obtained by the curve fitting of a set of cell potential (E) and current (i) data. Fig. 7 shows the calculated internal resistance of the MEAs. The internal resistances of the MEAs with added ZnO nanoparticles were lower than those without ZnO nanoparticles under the same operating temperature. This finding can be ascribed to the improved wettability of the catalyst layer, decreased ionic resistance, with ZnO

Table 3
MEA performances under different anode humidifier temperatures.

Operation temperature (°C)	MEA sample	Anode catalyst	Maximum current density (A cm^{-2})	Maximum power density (W cm^{-2})
25 °C–60 °C–65 °C	MEA0	20wt.% PtC	0.8379	0.1331
	MEA30	ZnO/PtC-30 s	1.2604	0.2022
	MEA60	ZnO/PtC-60 s	1.3515	0.2565
	MEA90	ZnO/PtC-90 s	1.1661	0.1864
45 °C–60 °C–65 °C	MEA0	20wt.% PtC	1.0551	0.1895
	MEA30	ZnO/PtC-30 s	1.5128	0.2726
	MEA60	ZnO/PtC-60 s	1.4519	0.2463
	MEA90	ZnO/PtC-90 s	1.1302	0.1778
65 °C–60 °C–65 °C	MEA0	20wt.% PtC	1.1229	0.2489
	MEA30	ZnO/PtC-30 s	1.5386	0.3127
	MEA60	ZnO/PtC-60 s	1.4737	0.3066
	MEA90	ZnO/PtC-90 s	1.1194	0.2381

Table 4
Saturation vapor pressure of water.

Temperature (°C)	Pressure (kPa)
25 °C	3.169
45 °C	9.589
65 °C	25.022

nanoparticle addition. MEA30 with 0.46 wt.% ZnO nanoparticles had the lowest internal resistance at the anode humidification temperatures of 45 °C and 65 °C. The excessive amounts of ZnO nanoparticles in MEA60 and MEA90 aggregated the particles, enhanced intrinsic resistance (electronic resistance), and poisoned the sulfonic groups of the Nafion membrane, which increased the internal resistance. The ionic resistance and the electronic resistance of MEA could be estimated to control the performance of single cell.

Overall, MEA60 had the highest power density of 0.26 W cm^{-2} among all the MEAs at 25 °C of anode humidifier temperature, which was 92.71% higher than that of MEA0. At 45 and 65 °C of anode humidifier temperatures, the maximum power densities of MEA30 were 43.85% and 25.78%, respectively, higher than those of the MEA0. These results indicated that the proper combination of suitable hygroscopic ZnO nanoparticles, uniformity of ZnO

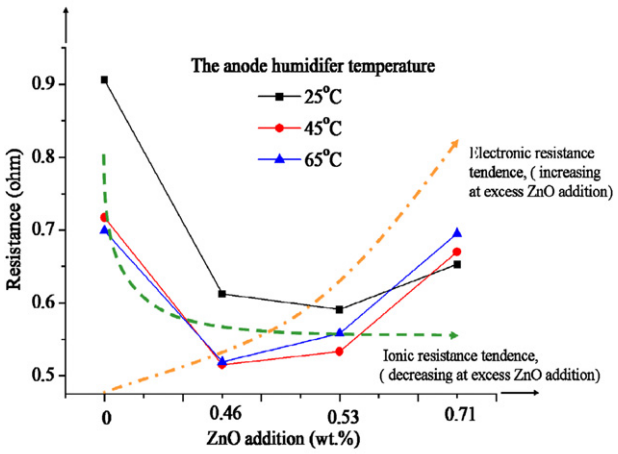

Fig. 7. Internal resistance vs. ZnO/PtC addition curves at different anode humidifier temperatures at the cathode humidifier temperature of 65 °C and cell temperature of 60 °C, containing the schematic curves of the combination effect of ionic resistance and electronic resistance.

nanoparticle distribution, and anode humidifier temperature yields the best MEA performance.

4. Conclusion

ZnO nanoparticles with spherical morphology and particle sizes from ca. 5–20 nm were well coated on PtC catalyst layer by sputter deposition, as revealed by SEM micrographs. XRD and SAD patterns confirmed the hexagonal structure of ZnO nanoparticles. The ZnO content of the ZnO/PtC nanocomposition increased with increased sputter deposition time. The water contact angles of the anode catalyst layers with added ZnO nanoparticles (0.46 wt.%, 0.53 wt.%, and 0.71 wt.%) became smaller ($41.17^{\circ\circ} \rightarrow {}^{\circ}33.08^{\circ\circ} \rightarrow {}^{\circ}13.75^{\circ}$). The hygroscopic ability of the ZnO/PtC composition improved. FTIR spectroscopy also demonstrated that the characteristic −OH wave number of the resulting ZnO/PtC composition showed a hygroscopic ability following increased ZnO addition. Among all MEA specimens with added hygroscopic ZnO nanoparticles to the anode catalyst layer, MEA60 with 0.53 wt.% ZnO nanoparticles exhibited the maximum current density of 60.71%, higher than that of the MEA0 without ZnO nanoparticles at the anode humidifier temperatures 25 °C. MEA30 with 0.45 wt.% ZnO nanoparticle exhibited maximum current densities of 43.80% and 36.60%, higher than those without ZnO nanoparticles at the anode humidifier temperatures 45 and 65 °C, respectively. Cell performance was determined by a competition mechanism between the positive effect wettability and negative effect electrical resistance of the anode catalyst layer, which great influenced the internal resistance. A balanced condition between the wettability and electrical resistance of the anode catalyst layer with added hygroscopic ZnO nanoparticles led to the best MEA performance.

Acknowledgments

The authors would like to thank the National Science Council of the Republic of China, Taiwan, for financially supporting this research under Contract no. NCS-99-2221-E-005-025-MY3.

References

[1] R. Beneito, J. Vilaplana, S. Gisbert, Int. J. Hydrog. Energy 32 (2007) 1544.
[2] J. Chen, T. Matsuura, M. Hori, J. Power Sources 131 (2004) 155.
[3] G. Hoogers, Fuel Cell Technology Handbook, CRC Press, Boca Raton, FL, 2003.
[4] K.B. Prater, J. Power Sources 61 (1996) 105.
[5] D.O.J. Murphy, G.D. Hitchens, D.J. Manko, J. Power Sources 47 (1994) 353.
[6] H.S. Chu, C.P. Wang, W.C. Liao, W.M. Yan, J. Power Sources 159 (2007) 1071.
[7] T. Vidakovi, M. Christov, K. Sundmacher, J. Electrochim. Acta 52 (2007) 5606.
[8] M.M. Saleh, T. Okajuma, M. Hayase, F. Kitamura, T. Ohsaka, J. Power Sources 164 (2007) 503.
[9] Philippe Bébin, Magaly Caravanier, Hervé Galiano, J. Membr. Sci. 278 (2006) 35.
[10] E.I. Santiago, R.A. Isidoro, M.A. Dresch, B.R. Matos, M. Linardi, F.C. Fonseca, Electrochim. Acta 54 (2009) 4111.
[11] F. Niepceron, B. Lafitte, H. Galiano, J. Bigarre, E. Nicol, J.-F. Tassin, J. Membr. Sci. 338 (2009) 100.
[12] A.K. Sahu, G. Selvarani, S. Pitchumani, P. Sridhar, A.K. Shukla, J. Electrochem. Soc. 154 (2007) B123.
[13] N.H. Jalani, K. Dunn, R. Datta, Electrochim. Acta 51 (2005) 553.
[14] S.Y. So, Y.J. Yoon, T.H. Kim, K.S. Yoon, Y.T. Hong, J. Membr. Sci. 381 (2011) 204.
[15] H.S. Thiam, W.R.W. Daud, S.K. Kamarudin, A.B. Mohammad, A.A.H. Kadhum, K.S. Loh, E.H. Majlan, Int. J. Hydrog. Energy 36 (2011) 3187.
[16] W. Dai, H.J. Wang, X.Z. Yuan, J.J. Martin, D.J. Yang, J.L. Qiao, J.X. Ma, Int. J. Hydrog. Energy 34 (2009) 9461.
[17] Y.S. Kim, F. Wang, M. Hickner, T.A. Zawodzinski, J.E. McGrath, J. Membr. Sci. 212 (2003) 263.
[18] M.L. Hill, Y.S. Kim, B.R. Einsla, J.E. McGrath, J. Membr. Sci. 283 (2006) 102.
[19] G. Alberti, M. Casciola, in: K.V. Peinemann, S.P. Nunes (Eds.), Membrane Technology, Membranes for Energy Conversion, vol. 2, Wiley–VCH, Weinheim, 2008.
[20] F. Croce, L. Settimi, B. Scrosati, Electrochem. Commun. 8 (2006) 364.
[21] M.V. Williams, H.R. Kunz, J.M. Fenton, J. Power Sources 135 (2004) 122.
[22] C.M. Lee, Y.H. Pai, F.S. Shieu, J. Electrochem. Soc. 156 (2009) B923.
[23] Y.H. Pai, J.H. Ke, H.F. Huang, C.M. Lee, J.M. Zen, F.S. Shieu, J. Power Sources 161 (2006) 275.
[24] U.H. Jung, K.T. Park, E.H. Park, S.H. Kim, J. Power Sources 159 (2006) 529.
[25] S. Vengatesan, H.J. Kim, S.Y. Lee, E. Cho, H.Y. Ha, I.H. Oh, S.A. Hong, T.H. Lim, Int. J. Hydrog. Energy 33 (2008) 171.
[26] W.K. Chao, C.M. Lee, D.C. Tsai, C.C. Chou, K.L. Hsueh, F.S. Shieu, J. Power Sources 185 (2008) 136.
[27] W.K. Chao, L.C. Chang, R.H. Huang, K.L. Hsueh, F.S. Shieu, J. Electrochem. Soc. 157 (2010) A1262.
[28] W.K. Chao, R.H. Huang, C.J. Huang, K.L. Hsueh, F.S. Shieu, J. Electrochem Soc. 157 (2010) B1012.
[29] A.K. Sahu, G. Selvarani, S. Pitchumani, P. Sridhar, A.K. Shukla, J. Appl. Electrochem. 37 (2007) 913.
[30] Anca Faur Ghenciu, Curr. Opin. Solid State Mater. Sci. 5 (2002) 389.
[31] G.W. Chen, S.L. Li, H.Q. Li, F.J. Jiao, Q. Yuan, Catal. Today 125 (2007) 97.
[32] L.Y. Li, D.L. King, Catal. Today 116 (2006) 537.
[33] T. Kim, Int. J. Hydrog. Energy 34 (2009) 6790.
[34] Y. Kawamura, K. Yamamoto, N. Ogura, T. Katsumata, A. Igarashi, J. Power Sources 150 (2005) 20.
[35] T. Shishido, Y. Yamamoto, H. Morioka, K. Takaki, K. Takehira, Appl. Catal. A: Gen. 263 (2004) 249.
[36] L.Y. Lin, H.J. Kim, D.E. Kim, Appl. Surf. Sci. 254 (2008) 7370.
[37] C. Badre, P. Dubot, D. Lincot, T. Pauporte, M. Turmine, J. Colloid Interface Sci. 316 (2007) 233.
[38] C. Badre, T. Pauporté, M. Turmine, D. Lincot, Superlattices Micro-struct. 42 (2007) 99.
[39] P. Sridhar, R. Perumal, N. Rajalakshmi, M. Raja, K.S. Dhathathretan, J. Power Sources 101 (2001) 72.
[40] R. Eckl, W. Zehtner, C. Leu, U. Wagner, J. Power Sources 138 (2004) 137.
[41] Y. Qiangu, T. Hossein, W. Junxiao, J. Power Sources 158 (2006) 316.
[42] N. Yousfi-Steiner, P.h. Mocoteguy, D. Candusso, D. Hissel, A. Hernandez, A. Aslanides, J. Power Sources 183 (2008) 260.
[43] B.M. Mahan, R.J. Myers, The Benjamin/Cummings, University Chemistry, Menlo Park, CA, 1987, p. 111.
[44] H.C. Tu, Y.Y. Wang, C.C. Wan, K.L. Hsueh, J. Power Sources 159 (2006) 1105.